# Adaptive pseudo-real-time forecasting of phytoplankton communities

*Trevor Page[1**], Paul J Smith[1,3], Keith J Beven[1], Ian D Jones[2], J Alex Elliott[2], Stephen C Maberly[2], Eleanor B Mackay[2], Mitzi De Ville[2] and Heidrun Feuchtmayr[2].*

*[1] Lancaster Environment Centre, Library Avenue, Lancaster University, Lancaster, LA1 4YQ, UK.*

*[2] Lake Ecosystems Group, Centre for Ecology & Hydrology, Lancaster Environment Centre, Library Avenue, Bailrigg, Lancaster, LA1 4AP, UK.*

*[3] ECMWF, Shinfield Park, Reading, RG2 9AX, UK*

*** Corresponding Author: t.page@lancaster.ac.uk*

**Key words**: Phytoplankton model, forecasting, data assimilation, Ensemble Kalman Filter, cyanobacteria, PROTECH.

## Abstract

Evaluation of the potential for forecasting of algal blooms using the phytoplankton community model PROTECH was undertaken in pseudo-real-time. This was achieved within a data assimilation scheme using the Ensemble Kalman Filter to allow uncertainties and model nonlinearities to be propagated to forecast outputs. Testing was done on two mesotrophic lakes in the English Lake district, which have differing depths and nutrient regimes. Some forecasting success was shown for chlorophyll *a*, but not all forecasts were able to perform better than a persistence forecast. There was a general reduction in forecast skill with increasing forecasting period but forecasts for up to four or five days showed noticeably greater promise than those for longer periods. Associated forecasts of phytoplankton community structure were broadly consistent with observations but their translation to cyanobacteria forecasts is challenging owing to functional similarities between species which may or may not be cyanobacteria.

. It was concluded that higher frequency in-lake chlorophyll *a* and nutrient observations should help to improve forecasts but it remains to be seen how far the forecasting system can be used to identify algal bloom conditions in this type of lake.

## 1 Introduction

Algal blooms are a global problem affecting water resources, recreation and ecosystems (Carmichael, 1992; Smith, 2003; World Health Organization, 1999). These problems are particularly acute when cyanobacterial species dominate because of the risk of toxin production that can cause adverse effects to humans and wildlife (Metcalf and Codd, 2009). In addition, water supply companies face associated problems such as poor taste and odour and, in extreme cases, high concentrations of algal-derived toxins which are costly to manage (Pretty *et al.*, 2003; Dodds *et al*., 2009; Michalak, 2016). Costs associated with implementation of management strategies are growing because of increased bloom frequency (Ho and Michalak, 2015) because of the effects of nutrient enrichment and climate change (Paerl and Huisman, 2008; Brookes and Carey, 2011; Rigosi *et al*. 2014). As a result, there is an urgent need for reliable predictions of algal bloom formation to enable timely management interventions.

Forecasting algal blooms in lakes is relatively new (Kim et al., 2014) but is increasingly becoming a requirement for lake and reservoir managers (Huang *et al*., 2013; Recknagel *et al*. 2014; Xiao *et al*., 2017) to help inform decisions regarding the most cost-effective management strategies. The fact that limmnology is rapidly becoming data-rich (Marcé *et al*., 2016; Xiao *et al*., 2014) means that effective real-time forecasts are increasingly more feasible. However, forecast simulations will be inherently uncertain for a number of reasons including input data resolution and simplifications in model process representation. These uncertainties will have implications for the accuracy and reliability of a forecast and therefore effort is required to allow for modelling uncertainty. Data assimilation (DA) is one approach to reducing forecast uncertainty, but has, to date, received relatively little attention for forecasting

phytoplankton community dynamics. There is hence a need to test different DA methodologies across different lake systems and different models.

There are still relatively few studies for operational lake forecasting systems and various approaches have been taken such as using: Ensemble Kalman Filter (EnKF; Evensen, 1994) schemes and physically-based simulation models (e.g. Allen *et al*., 2003, Huang *et al.* 2013 and Kim *et al,* 2014); evolutionary computation (Recknagel *et al.,* 2014; Ye *et al*., 2014); Lagrangian particle tracking model methods (Rowe *et al*., 2016); and using a combination of wavelet analysis and neural networks (Luo *et al*., 2011; Xiao *et al*., 2017). The EnKF has been developed to deal with highly non-linear model dynamics which cannot be represented well using the traditional Kalman Filter. Phytoplankton population dynamics are highly non-linear with multiple modes of behaviour that can respond rapidly to threshold-type effects and are prone to rapid changes in their physical and chemical environment (e.g. water temperature, light levels and available nutrients). This makes the EnKF a suitable choice to exploring algal bloom forecasting when coupled with a phytoplankton community model.

Here we assess our ability to make pseudo-real-time forecasts of phytoplankton communities in two lakes in the north west of England, which are prone to cyanobacteria blooms during the summer. Forecasts are made using a modified version of the phytoplankton community model PROTECH (Reynolds *et al*., 2001) within a DA scheme using the EnKF. The version of PROTECH employed is appropriate for this problem as it is intermediate in its complexity between physically-based coupled 3-dimensional hydrodynamic-biochemical models and more simplistic "black box models" which have both been used in this context. More complex models are extremely computationally expensive in forecasting (Huang *et al*., 2012; Recknagel, *et al*., 2014), such that only a limited number of ensemble members can be used (Kim *et al*., 2014); and simple black box models may not be able to represent phytoplankton community dynamics

driven by ecological strategies that are represented in phytoplankton community models such as PROTECH.

We aim to determine the efficacy of phytoplankton community forecast simulations, evaluate the EnKF as a DA strategy and investigate the ensemble size required for making consistent forecasts. Ultimately, success will rely on the modelling strategy being sufficiently effective to capture the necessary short-term phytoplankton community dynamics, given the available meteorological forecasts and limitations associated with driving data. Demonstrating the efficacy of the approach therefore requires a robust appraisal procedure with predictions tested qualitatively and quantitatively against appropriate benchmarks. This approach allows other pertinent questions to be investigated; namely, how does forecasting reliability diminish with time-scale of forecast and, most pertinently, what can be learnt from any forecasting failure regarding future model development and optimisation of monitoring strategies.

## 2 Methods

### 2.1 Study lakes

This study considers two lakes in the English Lake District of North West England with differing depths and nutrient regimes (Table 1). The catchments associated with each of the lakes are predominantly hill land, rough-grazed by sheep throughout the year and contain towns and villages that are tourist destinations and are hence associated with seasonal increases in lake nutrient inputs. Windermere is England's largest lake and comprises two basins connected at a shallow region approximately halfway along its main axis. The two basins are usually considered separately as they have different characteristics: both basins are monomictic and mesotrophic; the south basin was modelled in this study. Esthwaite Water is a small, generally monomictic and occasionally dimictic, lake that has been subject to eutrophication for many decades because of elevated phosphorus levels (Bennion *et al.,* 2000; Dong *et al*., 2012): cyanobacterial blooms are common in the summer to early autumn. Previous work has found that internal sources form

an important component of the P budget of the lake (Hall *et al*. 2000; Heaney *et al*., 1992 and Mackay *et al*., 2014).

***Table 1 Study Lakes and primary characteristics[§]***

| Name/location | Mean Depth (m) | Max. Depth (m) | Max. Length (m) | Volume ($m^3$) | Catchment Area ($km^2$) | Residence Time (days) |
|---|---|---|---|---|---|---|
| Windermere (South Basin) | 16.8 | 41 | 9300 | $1.06 \times 10^8$ | 230.5 | 100 |
| Esthwaite Water | 6.4 | 15.5 | 2500 | $5.97 \times 10^6$ | 17.1 | 100 |

*[§] Details from Ramsbottom (1976)*

## 2.2 Data

### 2.2.1 Forcing inputs: meteorological forecasts

The primary forcing inputs were meteorological forecasts provided by the European Centre for Medium-term Weather Forecasts (ECMWF) Ensemble Prediction System. The 10-day-ahead forecasts include an ensemble of 50 simulations from perturbed initial states (at 32 $km^2$ resolution) and stochastic perturbations of model parameters (see Buizza *et al.*, 1999 and Ollinaho *et al.,* 2016). The re-initialisation of model states in the ECMWF forecasting system is implemented using a higher resolution 3-hour forecast each day. As this re-initialisation is repeated each day, and as perturbations are random, there is no specific relationship between individual ensemble members in subsequent days. The forecast associated with each ensemble member was hence treated as independent from prior forecasts for this study. Daily averages of forecasts were used (i.e. the average of 3-hourly forecasts for days 1-6 and of 6-hourly forecasts day 6-10) for consistency with the daily timestep of PROTECH. Historic forecasts were obtained for 2008, 2009 and 2010 and used in pseudo-real-time. Given the scale of the forecast grid, each forecast variable was “downscaled” to local data as described in the next section.

### 2.2.2 Sampling meteorological forecasts

Downscaling relationships were developed for air temperature, wind speed, precipitation, cloud cover, relative humidity and solar radiation (Table 2). For air temperature a relationship was identified between forecasted temperatures and observed temperatures using linear regression. Residuals from this initial analysis helped identify an additional hysteretic relationship between forecasted and observed temperatures, which was attributed to a lake thermal effect; this effect was implemented as an additional correction for each day of the year. Similarly, wind speed was corrected using a linear correction factor coupled with an additional correction based upon wind direction; this was required owing to complex mountainous topography and lake-axis orientation. A wind-rose with sectors of 30 degrees was used to classify forecasted wind speeds and a sector-specific correction was applied. The uncertainty associated with the corrections was represented by fitting a gamma distribution to the data in each sector. All other variables (precipitation, cloud cover, relative humidity and solar radiation), were corrected using a correction multiplier identified using linear regression, without propagating the uncertainty in the relationship. The uncertain relationships for air temperature and wind speed were resampled as perturbations of the ensemble members allowing investigation of the effect of different ensemble sizes.

#### 2.2.3 Nutrient Inputs

Knowledge of diffuse nutrient inputs for the study lakes is relatively poor. Observations available were from approximately monthly frequency routine monitoring and did not cover all river inputs. Both lakes are also impacted by point sources from waste water treatment works (WwTW) and Esthwaite is subject to significant internal P fluxes (Mackay *et al*., 2014). Diffuse nutrient inputs and WwTW inputs (where included) were treated as reported by Page *et al*. (2017) and these inputs were modified by a multiplicative parameter included in the EnKF scheme (Table 3). For Windermere, upstream lake inputs of nutrients (and chlorophyll *a*) were treated as reported by Page *et al*. (2017) but were not included in the EnKF scheme.

133 ***Table 2 Forcing inputs and downscaling relationships***

| Model Inputs | Downscaling factor/relationship | Uncertainty sampled |
|---|---|---|
| Air Temp ($T_a$; K) | Windermere: 0.095($T_a^{§}$) + 279.75**<br>Esthwaite Water: 0.013($T_a^{§}$) + 280.16** | Y (Regression) |
| Solar Radiation (SR; $Wm^{-2}$) | 0.85 | N |
| Wind Speed (W; m $s^{-1}$) | 0.38¥ | Y (Gamma Dist.) |
| Relative Humidity (RH; %) | 1 | N |
| Cloud Cover (Cc; eighths) | 1.25 | N |
| Rainfall (R; mm) | 3 | N |
| Nutrient Inputs (P; N; $SiO_2$/ mg $m^{-3}$) | Section 2.2.3 | Y (Gamma Dist.) |

134 *$Ta^{§}$ is the forecast air temperature (K); ** see Section 2.2.2 for additional lake-effect correction; ¥ see Section 2.2.2 for additional*
135 *wind direction correction.*

136 **2.2.4 Data for assimilation**

137 Specific years where the observed data were of the highest frequency, were chosen to test the DA
138 strategy. High frequency data from the automatic lake monitoring systems (Madgwick *et. al*., 2006;
139 Mackay *et al*., 2014) were available and were aggregated to daily values. The variables used for DA are
140 listed in Table 3. The "observed" temperatures for the epilimnion ($T_e$) and hypolimnion ($T_h$) used to
141 compare with the modelled variables for these layers were calculated as volume-weighted averages of
142 thermistor chain data, using the simulated epilimnetic depth to delineate the hypolimnion and epilimnion.
143 The "observed" epilimnetic depth ($D_e$) was estimated using a density gradient method (e.g. see Read *et*
144 *al*., 2011). In addition to the automatic monitoring, routine monitoring was carried out at the buoy
145 location at a frequency of approximately every 14 days and included chlorophyll *a*, soluble reactive
146 phosphorus (SRP), dissolved inorganic nitrogen (DIN) and silica ($SiO_2$) (Table 3). These observations were
147 derived from a water sample at the buoy location integrated over 0-7 m depth (Windermere) or 0-5 m
148 depth (Esthwaite Water) (Maberly *et al*., 2010).

149

150 **2.3 Modelling methodology**

151 The modelling strategy employed was designed to represent the different facets of the forecasting
152 system as simply as possible to reduce computational burden, whilst retaining the requirement to

explicitly simulate phytoplankton community structure and, specifically, to estimate the likely concentrations of cyanobacteria from this structure. Thus, the catchment-lake system was simulated using a suite of models of differing complexity from purely data-based (statistically estimated) transfer function (TF) models and processed-based models which are consistent, in their complexity, with the available data. A schematic of how the models were combined in the forecasting system is presented in Figure 1 and each model is described in this section. The modelling system is structured around the rationale that epilimnetic depth must be estimated as accurately as possible so that the phytoplankton model, PROTECH, is more likely to provide good estimates of phytoplankton community structure; in PROTECH, community structure is simulated using functional algal types as classified by Reynolds (1988) as outlined in the next section. The simple conceptual model that estimates epilimnetic depth is a heat energy "balance" model that requires estimates of epilimnetic temperature and energy fluxes to the epilimnion, including those associated with river inflows and outflows.

***Table 3 Observed data assimilated in the EnKF scheme***

| Assimilated state | Frequency | Source |
|---|---|---|
| Epilimnetic Temperature ($^oC$) | Daily | buoy obs. |
| Hypolimnetic Temperature ($^oC$) | Daily | buoy obs. |
| Epilimnetic depth (m) | Daily | buoy obs. |
| Chllorophyll a (mg $m^{-3}$) | ≈14 days | Monitoring |
| Nutrient Inputs (SRP; N; $SiO_2$ / mg $m^{-3}$) | ≈14 days | Monitoring |

The TF models, epilimnetic depth model and PROTECH are run sequentially; the TF and epilimnetic depth models provide forecast estimates of river flow, epilimnetic depth, epilimnetic temperature and hypolimnetic temperature as inputs to PROTECH. Data assimilation is employed for the two primary models (the epilimnetic depth model and PROTECH) using two separate EnKF schemes that assimilate observations at different intervals; the epilimnetic depth model scheme assimilates epilimnetic depth and epilimnetic temperature estimates as well as hypolimnetic temperature estimates on a daily basis and the scheme for PROTECH assimilates nutrient and chlorophyll *a* concentrations approximately every 14 days.

### 2.3.1 The PROTECH model

PROTECH (Reynolds *et al*., 2001) is a lake phytoplankton community model that runs on a daily time-step. It is a 1-dimensional model where the lake is represented by horizontal layers. In the model representation all layers are assumed to be fully mixed throughout the epilimnion. River inputs drive fluxes of diffuse nutrients as well as the flushing of phytoplankton. Upstream lake inputs are treated as river inputs but are given the phytoplankton concentrations associated with the upstream lake, where data are available.

Underwater light for model layer *i* is calculated using:

$$l_i = Isurf.e^{(-\varepsilon.d_i)} \quad (1)$$

Where: *Isurf* is the daily surface light flux, *d* is the depth from the lake surface, $\varepsilon$ is the light extinction coefficient resulting from the sum of lake-specific abiotic water attenuation ($\varepsilon_b$) and the extinction of light associated with the concentration of phytoplankton at each timestep multiplied by the parameter $\varepsilon_a$. In the layers from the surface to the epilimnetic depth, the available light is represented by the geometric mean of the epilimnetic layers and hence assumes that phytoplankton spend an equal time in each layer at each timestep. Phytoplankton population dynamics are simulated using the following equation which describes the change in chlorophyll *a* concentration (*X*) of each phytoplankton species selected to represent the algal community (Reynolds 2001):

$$\frac{\Delta X}{\Delta t} = (r' - S - G - F).X \quad (2)$$

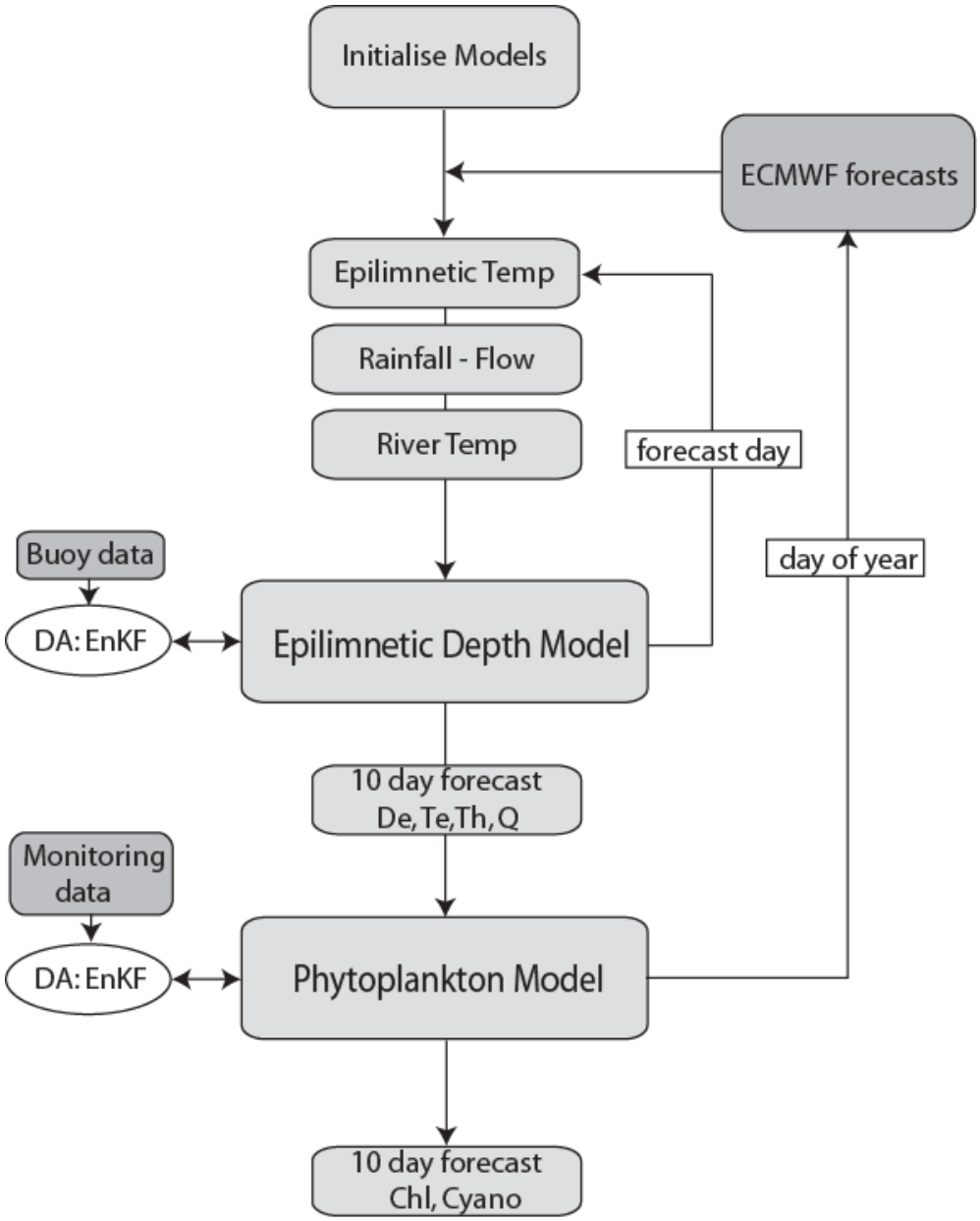


192

193 *Figure 1. Schematic diagram of the forecasting system. The schematic shows sequential model*
194 *input-output structure and DA strategy. De is epilimnetic depth; Te is epilimnetic temperature; Th*
195 *is hypolimnetic temperature, Q is lake inflow/outflow and Chl and Cyano are the concentration of*
196 *total phytoplankton chlorophyll a and cyanobacterial chlorophyll a respectively.*

where $r'$ is the growth rate, *S* is settling loss, *G* is a grazing loss and *F* is the loss due to flushing. The growth rate is defined for each layer using:

$$r' = \min\{r'_{(\theta)}, r'_{(P)}, r'_{(N)}, r'_{(Si)}\} \quad (3)$$

where $r'_{(\theta,I)}$ is the growth rate at a given temperature ($\theta$) and daily photoperiod (*I*) and $r'_P$, $r'_N$, $r'_{Si}$ are the growth rates determined by phosphorus, nitrogen and silica concentrations. The final growth rate ($r'_{cor(\theta,I)}$) is a corrected rate allowing for dark respiration using equation 4. This is required as the model growth equations are net of basal metabolism but not dark respiration burden.

$$r'_{corr(\theta,l)} = R_{d(\theta)}.r'_{(\theta,l)} - \left(1 - R_{d(\theta)}.\right).r'_{(\theta,l)} \quad (4)$$

Where $R_{d(\theta)}$ is the dark respiration rate at temperature $\theta$. The phytoplankton used for this study are presented in Table Supp. 2.

PROTECH simulates the dynamics of the species chosen to represent the algal community of a given lake. Species are represented by their morphology, nutrient requirements (i.e. silica requirement and nitrogen fixing ability) and their vertical movement strategies. The number of species simulated is nominally eight (although unlimited) and they are chosen to represent the dominant functional types of the system. Simulations hence represent the behaviour of the functional algal community rather than the dynamics of specific species. The C-S-R functional phytoplankton classification of Reynolds (1988) is used to classify phytoplankton into morphologically defined groups relating to broad ecological strategies. The primary groups are: C-types, which are invasive, ecological pioneers that are small with high surface-to-volume ratios (e.g. Chlorella, and Plagioselmis); S-types which are 'stress tolerators' that tolerate relatively low nutrient availability and strong stratification (e.g. Woronichinia, Microcystis and Oocystis); and R-types which can harvest sufficient light at low levels to be able to maintain growth and are hence tolerant of well-mixed, intermittently insolated environments (e.g. Asterionella, Aulacoseira and Oscillatoria). Also

219 important for the lakes studied here, are CS-types, whose characteristics are intermediate between those
220 of C and S species (e.g. Dolichospermum, Aphanizomenon and Ceratium) and CSR-types (e.g.
221 Cryptomonas) that are intermediate between C-, S- and R-types.

222 **2.3.2 Epilimnetic depth model**

223 As a way of reducing computational burden, a simplified representation of lake thermal structure was
224 employed to estimate epilimnetic depth ($D_e$). The simplified model works on the basis of *independent*
225 estimates of epilimnetic temperature and lake heat energy fluxes. The estimate of epilimnetic
226 temperature ($T_e$) uses a TF model (see Section 2.3.3) with inputs of air temperature ($T_a$), solar radiation,
227 wind speed (Ws) and $D_e$. Air temperature solar radiation and wind speed are derived from the forecasts
228 and $D_e$ estimates are from the previous simulation timestep. The independent estimates of heat energy
229 fluxes are calculated using the PROTECH energy flux function (see Reynolds *et al*., 2001) for each timestep
230 using $T_e$, river temperature and flow magnitude, day length, cloud cover, $T_a$, Relative Humidity and Ws.

231 These two independent estimates are "balanced" to obtain hypolimnetic volume ($V_h$) using:

232 $$V_h = \frac{E_{\Delta T}}{\Delta T . C_w . \rho_w} \quad (5)$$

233 where, $E_{\Delta T}$ is the heat energy associated with $\Delta T$ (the difference between $T_e$ and the hypolimnetic
234 temperature, $T_h$), $C_w$ is the specific heat capacity of water, $\rho_w$ is the density of water. Equation 5 is solved
235 to find $V_h$ where: $\Delta T . C_w . \rho_w . V_h \approx E_{\Delta T}$. Subsequently, the epilimnetic volume ($V_e$) and hence epilimnetic
236 depth ($D_e$) are estimated by difference:

237 $$V_e = V_t - V_h \quad (6)$$

238 where $V_t$ is the total lake volume. The requirement for $\Delta T$ is satisfied by calculating $T_h$ using:

239 $$T_h = \frac{E_{th}}{C_w . \rho_w . V_t} \quad (7)$$

where: $E_{th}$ is the "background" heat energy in the lake (associated with $T_h$ and $V_{t,}$ *as defined by Eqn. 7*). During the forecast period, $E_{th}$ remains at its previous value until updated during the data assimilation step. This treatment of $E_{th}$ neglects the explicit downward transfer of energy from $E_{\Delta T}$ to $E_{th}$ for forecasting and assumes that these are negligible over this timescale: energy is, however, explicitly transferred downwards each time temperatures are updated during data assimilation. The sequence of calculations for each forecast timestep is:

1. Estimate lake surface temperature using TF model
2. Update $E_{\Delta T}$
    I. Radiative energy fluxes
    II. River/upstream lake fluxes
        - Estimate river input volume using TF model
        - Estimate river temperature using TF model
        - Assume Upstream lake temperature = modelled lake temperature
    III. If $E_{\Delta T} < 0$ loose energy from $E_h$ (minimum energy set to 0°C)
3. Estimate $T_h$ from $E_{th}$
4. If $E_{\Delta t} > 0$ and If $T_e - T_h$ is greater than a threshold parameter (nominally set to 1°C) estimate epilimnetic depth by solving for the volume of water required to match $E_{\Delta T}$ given $\Delta T$: subsequently estimate $V_e$ and hence $D_e$ by difference.

### 2.3.3 Transfer Function models

Transfer Function (TF) models were used for estimating lake surface temperature, river temperature and river inflows and outflows. Each model is a discrete-time TF identified directly from the available data. Both the model structures and parameters were identified using the Refined Instrumental Variable (RIV) algorithm (Young, 2015) implemented within the CAPTAIN Toolbox for Matlab™ (Taylor *et al.*, 2007). The

resulting model structures and parameter values are presented in Section (Supp. 1) and are either single input- or multi-input, single-output first order models of the general form:

$$y_t = \frac{B_1(z-1)}{A(z-1)} U_1 + \frac{B_2(z-1)}{A(z-1)} U_2 + \cdots \frac{B_n(z-1)}{A(z-1)} U_n \quad (8)$$

where, $y_t$ is the variable being estimated at time *t*, $U_{1\text{-}n}$ are model input vectors, $A(z-1)$ and $B_n(z-1)$ are the model coefficients (polynomials in the backward shift operator: defined by $y_t z^{-1} = y_{t-1}$) that number 1 to $n$ in the case of $B$ but note that in this form for MISO (multi-input single-output) TF the denominator ($A$) is common to all $n$ TF elements.

### 2.3.4 The Ensemble Kalman Filter

The EnKF is a sequential Monte Carlo method which uses a stochastic ensemble of model simulations, and stochastic forcing, to propagate estimates of model states and (or) parameter values between assimilation timesteps. As the ensemble of model simulations is used in place of the linear propagation of an error covariance matrix (as in the traditional Kalman Filter), non-linear model dynamics are retained during model evolution and uncertainties are represented by the variation of the ensemble. When observations are available, each ensemble member is updated individually using a linear update equation (Eqn. 9) which relies on the assumption that the relationship between states and parameters can be described by multivariate Gaussian distributions. Rather than resampling the posterior distributions of the updated ensemble, the EnKF uses each updated ensemble member such that some of the non-Gaussian properties of the forecast are retained (Evenson, 2009). The procedure for the scheme is as follows:

1. The EnKF is initialised with an *N* number ensemble size, sampling states and parameters from *a priori* specified distributions (see below for specific details of this study) and *N* simulations for the forecast period are carried out. Where parameters are varied as part of the EnKF scheme, they are appended to the state matrix to give a state-parameter matrix.

2. When observed data are available for assimilation:

I. Apply a linear covariance inflation factor $(I)$ to each of the $i$ states and parameters to reduce the tendency for low ensemble covariance and for spurious correlations associated with small ensemble size (Anderson, 2007; Anderson and Anderson, 1999; Evenson, 2009):

$$\varphi_{j,i}^{a} = I.\left(\varphi_{j,i}^{a} - \overline{\varphi_{i}^{a}}\right) + \overline{\varphi_{i}^{a}} \quad (9)$$

II. Generate *N* perturbations of the observations $(Y)$; it is essential that the uncertainty associated with the observations is sampled from a distribution with mean equal to the observed value and covariance ($P^{e}$) to avoid bias in the update (Evenson, 2009) and to reduce further the tendency for the updated ensemble to have very low covariance (Moradkhani *et al*., 2005).

III. Update the model states and parameters individually for the $j^{th}$ ensemble member. This is done proportionally to the deviation of the states in the forecasted state-parameter matrix $(\varphi^{f})$ from the vector of perturbed observation$s$ and the Kalman gain matrix $(K)$: note that the timestep suffix is omitted for clarity in the following equations:

$$\varphi^{a} = \varphi^{f} + K(Y) - H\varphi^{f}) \quad (10)$$

where, $\varphi^{a}$ is the vector of updated states/parameters and $H$ is a matrix that maps the model states to the observed sates. The appended parameters are updated using the cross-covariance between the predicted states and parameters. The Kalman gain matrix is calculated using:

$$K = P_{\varphi}^{f} H^{T}(H\left(P_{\varphi}^{f}\right)H^{T} + P^{e})^{-1} \quad (11)$$

where, $P_{\varphi}^{f}$ is the covariance matrix for the ensemble of forecasted state-parameter matrix.

IV. Apply any constraints on states and (or) parameter distributions (e.g. to keep them within physically reasonable ranges). This was implemented using a resampling scheme where if any state/parameter violated specified constraints (Table 4), the ensemble was resampled using a truncated distribution for that state/parameter in conjunction with a Gaussian copula to retain the ensemble's covariance structure.

V. Make *N* number of simulations for the next forecast period using the updated state-parameter matrix.

### 2.3.5 Ensemble Kalman Filter scheme: Epilimnetic model

As the epilimnetic model is very simple, all the main model states were used in the EnKF scheme. The states $T_e$, $T_h$ and $D_e$ were updated using a daily assimilation frequency for the epilimnetic depth model. The "observed" values of these states are those estimated and described above.

### 2.3.6 Ensemble Kalman Filter scheme: PROTECH

The choice of states and parameters included in the PROTECH EnKF scheme was made based on uncertainty and sensitivity analyses reported by Page *et al.* (2017). The Page *et al*., study, which included the lakes studied here, identified that the main challenges for forecasting as uncertainties associated with: representing phytoplankton exposure to light and nutrient inputs (particularly phosphorus). The DA scheme was therefore defined to include the main model states, SRP, DIN, $SiO_2$ and chlorophyll *a*, as well the parameters associated with modifying nutrient inputs and underwater light (Table 4). These were updated at an approximately 14-day frequency set by the monitoring data. For Windermere both point source ($WwTW_f$) and diffuse SRP inputs ($P_{fact}$) parameters were included in the DA scheme; for Esthwaite

Water only the parameter modifying the diffuse SRP inputs was included as simulations which included a simplified representation of sediment-derived SRP inputs did not provide improved results (these results are not reported here).

To investigate the effect of ensemble size and to determine an acceptable ensemble size for the current applications, ensemble member (EM) size was increased sequentially, using the scenarios EM50, EM100, EM200, EM300 and EM400 (where the suffix is the size of the ensemble), until the forecast simulations appeared consistent. These scenarios were generated by resampling the downscaled ECMWF forecast distributions as described above and were used to force the suite of models used. For each of the forecast scenarios, the error associated with the assimilated data and the variance inflation factors were "optimised" manually to provide the best results. For consistency, and in the spirit of the pseudo-real time treatment of the forecast simulations, the variance inflation factors were kept consistent across all lake-years considered. For each of the assimilated variables, the variance was assumed to be proportional to the magnitude of the variable of interest using a percentage. Additionally, a minimum variance was applied to reduce the impact of very small observed values (e.g. where hypolimnetic SRP values are observed to be very low or within the limit of detection) where the associated low variance would falsely indicate low uncertainty.

***Table 4. States and parameters included in the ENKF scheme***

| State/Parameter | Acceptable range | Observational error (%) | Initial distributions (uniform)** |
|---|---|---|---|
| Epilimnetic Temp. ($T_e$, $^0$C) | 2-25 | 5 | 5.5-7 (W); 4-6(E) |
| Hypolimnetic temp. ($T_h$, $^0$C) | 2-25 | 10 | 5.5-7 (W); 4-6(E) |
| Epilimnetic depth ($D_e$, m) | 0.5-Lake max. depth | 5 | 41 (W); 15.5(E) |
| Chlorophyll *a* (mg m$^{-3}$) | 1e$^{-6}$-1e$^{3}$ | 10 | 3-4.5 (W); -4.5-6 (E) |
| Background light extinction ($\varepsilon_b$, $m^{-1}$) | 0.15-0.9 | N/A | 0.15-0.6(W); 0.45-0.75(E) |
| Epilimnetic P conc. ($P_e$ ,mg m$^{-3}$) | 1e$^{-6}$-1e$^{4}$ | 25 | 10-20(W); 8-15(E) |
| Epilimnetic DIN conc. ($N_e$,mg m$^{-3}$) | 1e$^{-6}$-1e$^{4}$ | 25 | 400-700(W); 500-1100(E) |
| Epilimnetic $SiO_2$ conc. ($Si_e$,mg m$^{-3}$) | 1e$^{-6}$-1e$^{4}$ | 25 | 1500-2500(W); 2000-2500(E) |
| Diffuse P input multiplier ($P_f$, dimensionless) | 0.05-7 | N/A | 0.01-1.5 |

| | | | |
|---|---|---|---|
| Diffuse DIN input multiplier ($N_f$, dimensionless) | 0.1-3 | N/A | 0.5-1.2 |
| Diffuse $SiO_2$ input multiplier ($Si_f$, dimensionless) | 0.1-3 | N/A | 0.5-1.2 |
| Point source P input multiplier ($WwTW_f$, dimensionless) | 0.01-2 | N/A | 0.1-1.4 |

****** Where distributions are different for each lake W = Windermere; E = Esthwaite Water

### 2.3.7 Assessing forecast skill

Different studies have used different benchmarks to evaluate the goodness of fit of forecasts (*forecast skill*), which are often determined by their aims. Studies tend to use either some form of "reference" simulation or simulations that do not assimilate any observations (sometimes called "climatology") which serve to quantify the DA effect (e.g. Allen *et al.,* 2003 and Kim *et al.*, 2014) or solely a measure of the goodness-of-fit to observations (e.g. the coefficient of determination, $R_T^2$). Here, as our aim was to assess the value of the model for operational forecasting, we used a more stringent *persistence forecast* (e.g. see Stumpf *et al*., 2009) which uses the most recent observations as the forecast for each *forecast timestep* until the next observation becomes available. In the sections below, the forecast skill was assessed using a persistence forecast for the entire annual timeseries and for the chlorophyll *a* forecast for which we have the most confidence in the observations. The goodness of fit of the benchmark and the simulated chlorophyll *a* forecasts are determined using the root-mean-square error (RMSE) as a measure. For the epilimnetic depth model, and other sub-models (i.e. TF models), goodness of fit is discussed more generally by comparison with observations using the coefficient of determination ($R_T^2$). Assessment of the forecasts of phytoplankton community structure is made qualitatively as we have a significantly lower confidence in the absolute value of the observations.

## 3 Results and discussion

### 3.1 TF model results

Transfer function models were identified for epilimnetic temperature, river temperature and river inflows and outflows and all models provided good fits to the observed data during model identification: $R_T^2$ values were between 0.86 and 0.98 (Supp. Table 1). Model identification was carried out for the entire period of data available (see Supp. 1) such that they were not year specific models. As detailed above, in each case the models were used to forecast their respective variable deterministically.

### 3.2 Forecasting epilimnetic depth and the phytoplankton community

#### 3.2.1 Epilimnetic depth forecasts

Epilimnetic depth forecast estimates were made for 2008-2010 for Windermere and 2008 and 2009 for Esthwaite Water within the parallel EnKF scheme. Although very simplistic, the epilimnetic depth model provided reasonable forecasts of epilimnetic depth when compared to those estimated from observations. For both lakes, the forecasts were stable and consistent using the smallest ensemble size of 50 using a variance inflation factor of 1.25. Simulations for Windermere were better than for Esthwaite Water ($R_T^2$ of 0.85 and 0.75 respectively for a 10-day-ahead forecast; Figs. 2a and 2b) and there were short periods with significant deviations from the 'observed' depths in both cases. Simulation of the timing of temporary stratification events at the beginning of the year was problematic for both lakes and simulations tended towards overly rapid mixing during autumn turnover, particularly for Esthwaite Water. Where significant deviations exist, they have the potential to reduce the forecast skill and therefore need to be improved, although, importantly, epilimnetic depth estimates for much of the high cyanobacterial bloom risk periods (i.e. during periods of strongest stratification) are reasonable. Given these results, the epilimnetic depth estimates for Windermere appear to be adequate out to 10-days-ahead but for Esthwaite they appear to be adequate for a much shorter lead time; for example, the 3-day-ahead forecast is a much better fit with an improved $R_T^2$ of 0.81 (Fig. 2c). The adequacy of these estimates is assessed

more formally in association with the phytoplankton forecasts in comparison to the persistence forecast in the next section.

### 3.2.2 Chlorophyll *a* forecasts

For all lake-years, multiple runs of the EM50 Forecasts gave inconsistent simulations and a higher EM size was required. Forecasts for Windermere tended towards stability between the EM100 and EM200 scenarios (Fig. 3), which is an ensemble size consistent with previous work with relatively complex models (e.g. Evensen, 1994 and Allen *et al*., 2003). For Esthwaite Water, however, a higher ensemble size appeared to be required with a size of around 400 giving consistent simulations (Fig. 4). Subsequently, in the following, results presented for Windermere and Esthwaite Water are associated with the EM200 and EM400 scenarios respectively. In all cases, the manually "optimised" variance inflation factor was kept consistent for all lake years at a value of 1.1.

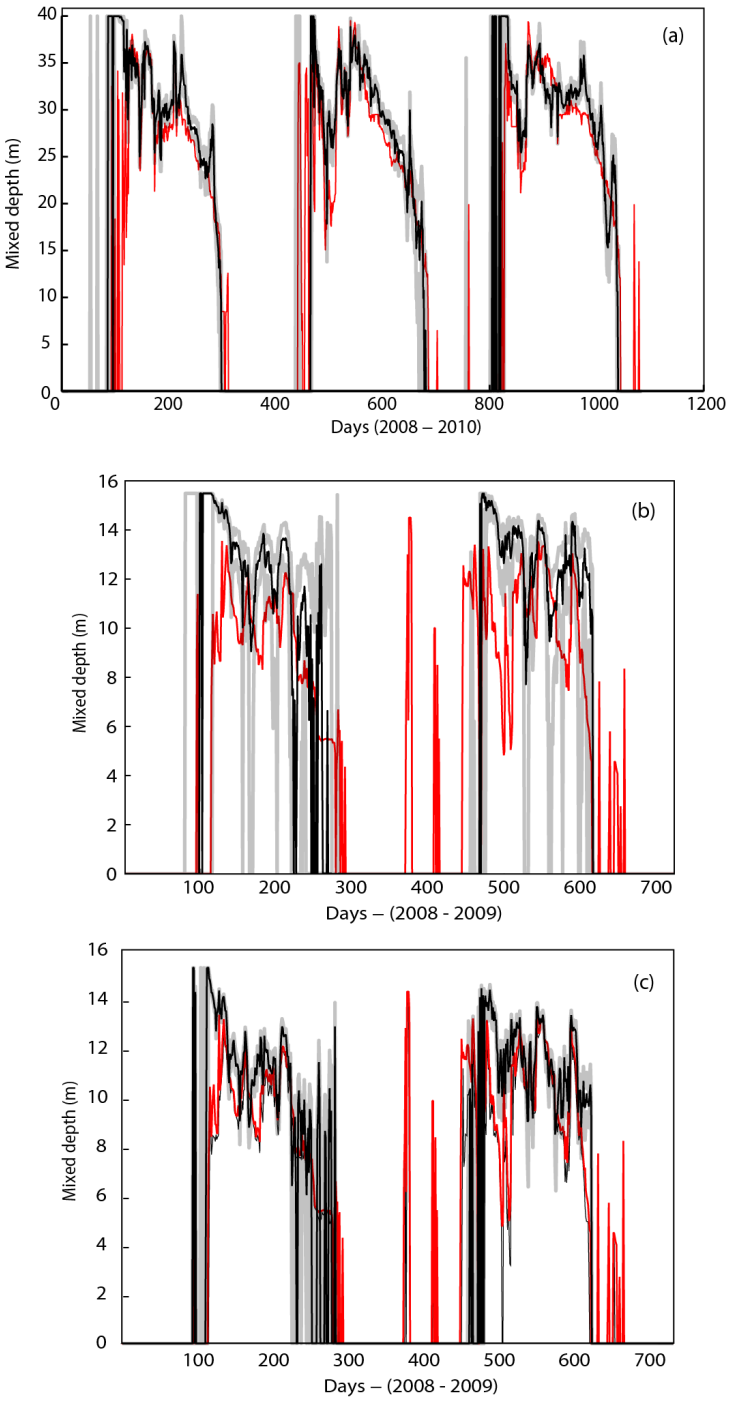


404

405 *Figure 2. Simulated and measured epilimnetic depth. Results shown for (a) Windermere 2008-2010*

406 *10-day-ahead, (b) Esthwaite Water 2008 and 2009 10-day-ahead and (c) Esthwaite Water 2008*

407 *and 2009 3-day-ahead: "observed" epilimnetic depth (red line), 50$^{th}$ percentile of the ensemble of*

408 *simulated epilimnetic depth (black line) and 5$^{th}$ and 95$^{th}$ percentiles (grey lines).*

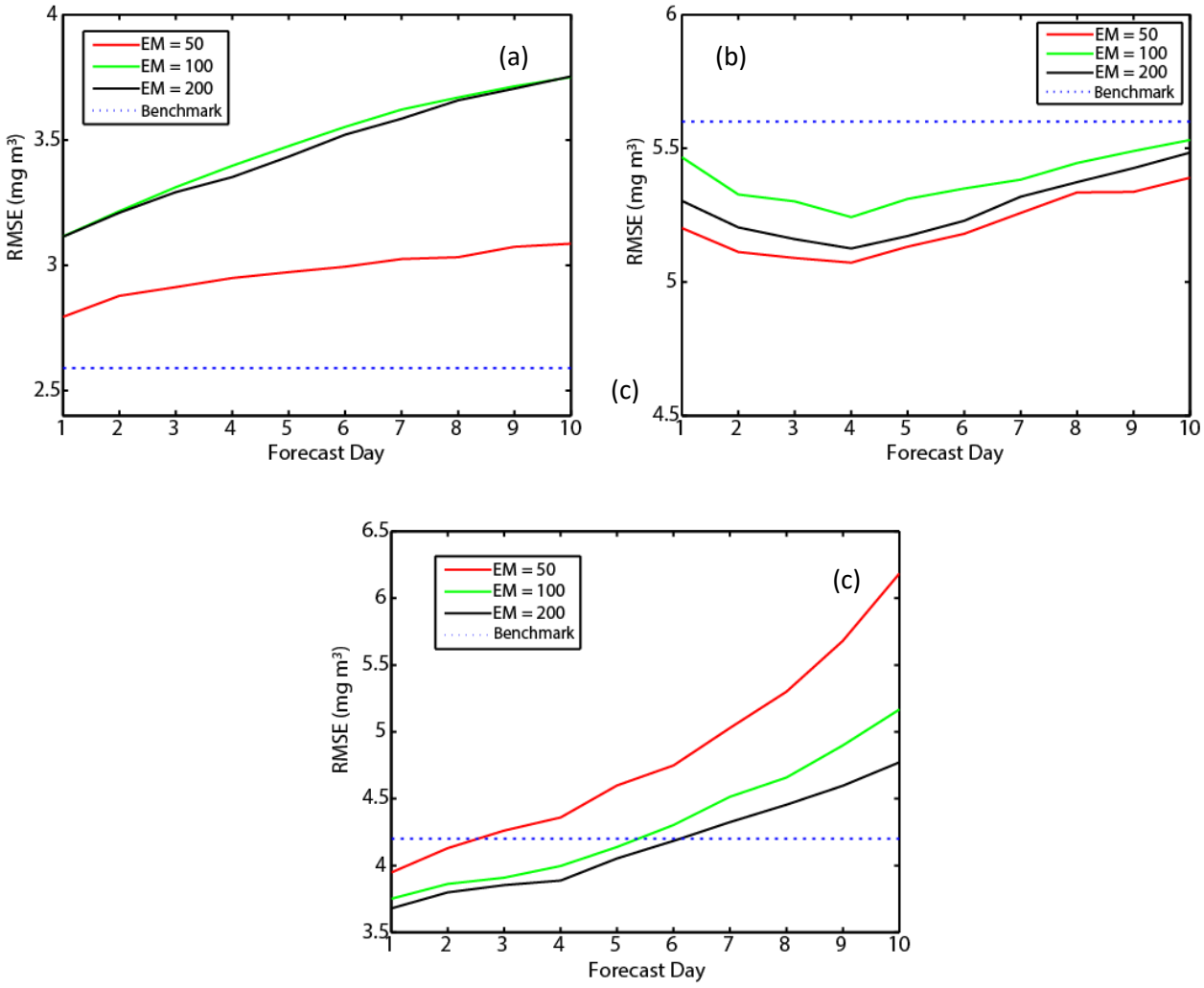


*Figure 3. Chlorophyll a forecast skill for the differing ensemble size scenarios. Results are shown for (a) Windermere 2008, (b) Windermere 2009 and (c) Windermere 2010, compared to the benchmark persistence forecast. Note that lower ensemble sizes can give "randomly" better forecast performance (e.g. EM = 50 in pane (a))*

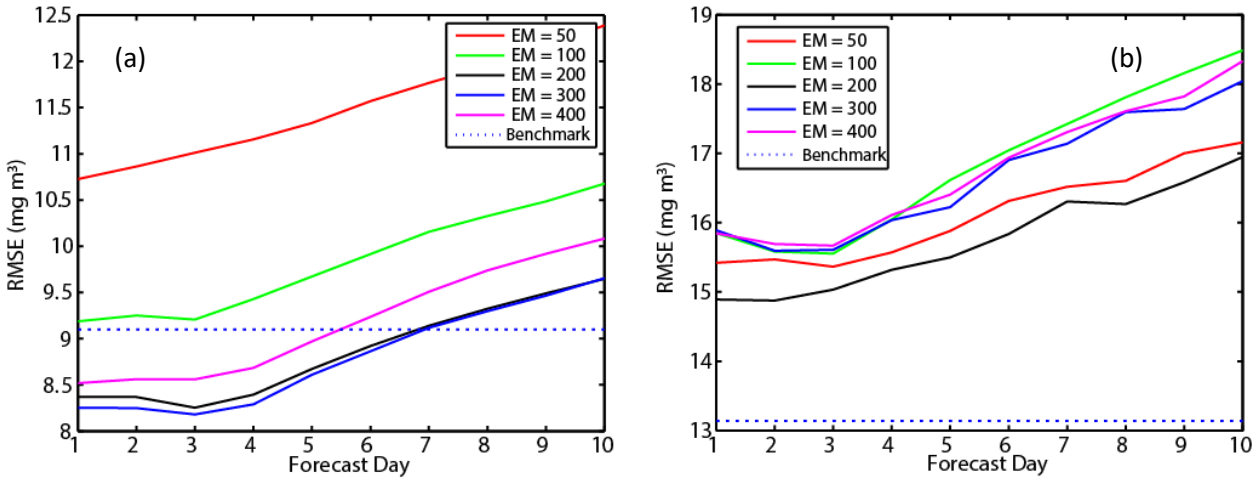


*Figure 4. Chlorophyll a forecast skill for the differing ensemble size scenarios. Results are shown for (a) Esthwaite Water 2008 and (b) Esthwaite Water 2009, compared to the benchmark persistence forecast.*

Although forecast simulations for Windermere appear to be relatively good visually (e.g. see Fig. 5 below), they were not always an improvement on the persistence forecasts (Fig. 3). For 2008, the persistence forecast was better than simulated forecasts for all lead times. Conversely, simulated forecasts were better than the persistence forecasts for all lead times for 2009. A lead time of approximately 6 days or less was an improvement on the persistence forecast for 2010 simulations.

For Esthwaite Water, forecasts simulations were not as good as those for Windermere (Fig. 5), which is consistent with previous work using PROTECH for these lakes (Page *et al*., 2017). The forecasts for 2008 were, however, still better than the persistence forecast out to about 5 days ahead (Fig. 4a), but were always worse than the persistence forecast for 2009 (Fig. 4b). The poorer fits for Esthwaite Water are likely to be a result of the complex uncertainties associated with the timing and magnitude of SRP inputs as well as the poorer simulation of epilimnetic depth reported above. In Esthwaite Water, during the period where P limitation dominates phytoplankton growth, it is very difficult to represent SRP fluxes

434 appropriately, even when a representation of sediment-derived SRP fluxes was included (the addition of
435 representation of sediment-derived SRP did not improve forecasts owing to interaction between sources
436 of P: this work is not reported here). The difficulties associated with representing SRP fluxes was helped
437 to some degree by the DA, but remain problematic during times where very low concentrations are
438 present in the epilimnion; at these times, the correlations within the Kalman gain matrix would need to
439 be very well-represented to provide appropriate updates to both epilimnetic SRP concentrations and SRP
440 fluxes simultaneously. The difficulties associated with these updates are compounded by the relatively
441 low frequency of assimilation timesteps. Subsequently, even with relatively large ensemble sizes, the
442 correlations within the Kalman gain matrix have the potential to be spurious. This is not unexpected as
443 the lake system is highly dynamic and non-linear and, perhaps most importantly, the relationships
444 between the states (and parameters in some cases) are not always consistent (e.g. when the nutrient
445 states are not limiting they may have no relationship with the phytoplankton state). The temporal
446 evolution of the nutrient parameter values (modified within the DA scheme) that change SRP fluxes were
447 consistent with these uncertainties and did not show any consistent structure. Given these difficulties,
448 assimilation of higher resolution nutrient observations may be one of the most important for improving
449 forecasts. Conversely, for both Windermere and Esthwaite Water, improvement of forecasts was made
450 by the modification of the background light extinction parameter, $\varepsilon_b$, within the DA scheme: its evolution
451 over the simulation periods was relatively consistent for each of the years considered (Fig. 6) and reflects
452 known simulation artefacts previously reported (Page *et al*., 2017).

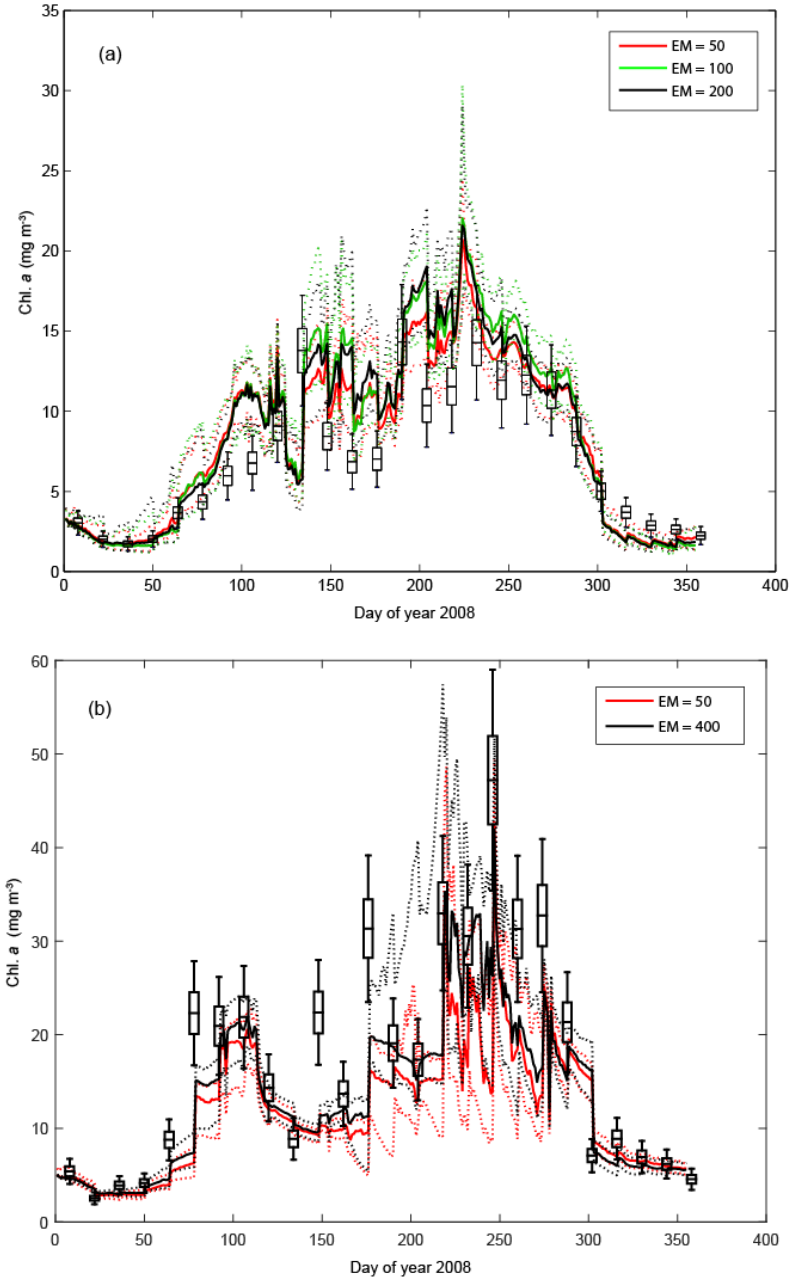


453

454 *Figure 5. Measured and forecast phytoplankton chlorophyll* a *in the two lakes during 2008. Results*
455 *show concatenated forecasts for: (a) 10-day-ahead for Windermere 2008 for ensemble member*
456 *sizes (EM) of 50, 100 and 200; (b) 5-day-ahead for Esthwaite Water 2008 for ensemble member*
457 *sizes (EM) of 50 and 400. Solid lines are 50$^{th}$ percentile of ensemble and dotted lines are 5$^{th}$ and*
458 *95$^{th}$ percentiles.*

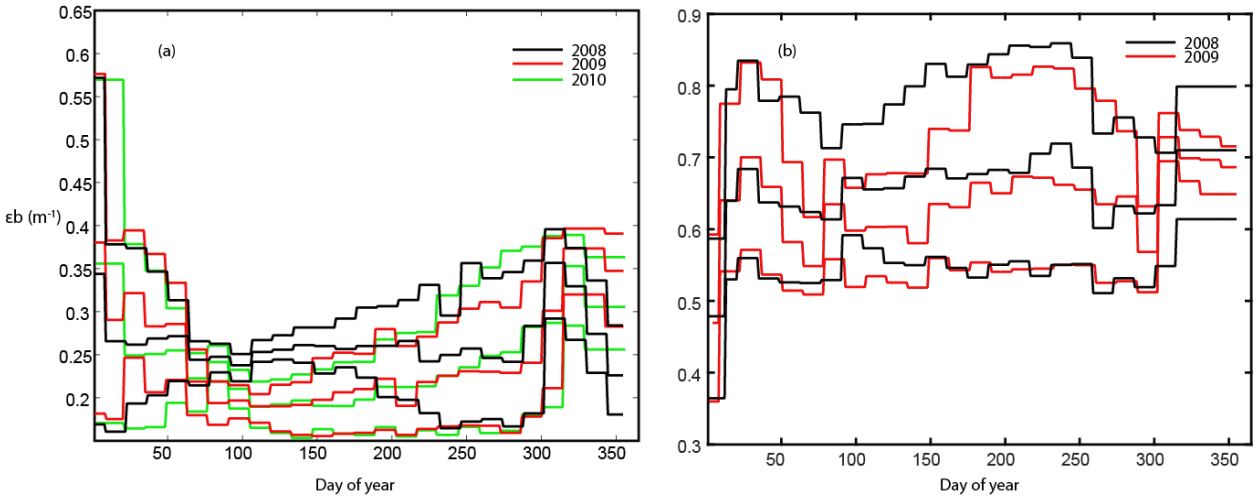


*Figure 6. The evolution of the background light extinction coefficient parameter ($\varepsilon_b$). Results are shown for (a) Windermere 2008, 2009 and 2010 and (b) Esthwaite Water 2008 and 2009. The three lines in each colour are the 5$^{th}$, 50$^{th}$ and 95$^{th}$ percentiles of the EM200 and EM400 ensembles respectively.*

### 3.2.3 Forecasting phytoplankton community structure

Forecasts of species representing the phytoplankton community structure were made without direct constraint within the DA scheme. Simulations were, however, indirectly constrained by the assimilation of mixed depth, chlorophyll *a* and nutrients and hence are reliant on the ability of PROTECH simulations to represent phytoplankton community structure where abiotic conditions for phytoplankton growth are simulated adequately. They are also reliant on whether or not the algal species chosen to represent the community are adequate (Elliott, 2010, 2012; Page *et al.,* 2017).

Forecasts of community structure are assessed here using simulations of R- and CS-types functional groups as they dominate our study lakes. Observations to which they are compared are estimated using "counts" of algal species classified into the same functional groups. These "count" data are associated with significant uncertainty in terms of the absolute biovolume of each species (and hence functional

type) because of errors, which are difficult to quantify, associated with sample heterogeneity, counter fatigue and between-counter variation (Thackeray et al., 2012) as well as uncertainty associated with conversion from sample "counts" to biovolume and subsequently to chlorophyll *a*. Accordingly, we used the relative abundance of each functional type for each observation timestep to partition the observed chlorophyll a concentration. Given these uncertainties, we estimated the sampling/analytical error to be +/- 25% and the overall error to be +/- 50% in accordance with Page *et al*. (2017).

A comparison of the uncertain observations of R- and CS- functional types are presented in Fig. 7 where it can be seen that for most lake-years the overall pattern of the simulations are consistent with the observations. There are some periods where the simulations are not consistent, which are associated primarily with the period of transition between the early blooms of R-type species and succession by CS-types (approximately between days 100 and 200). This pattern can clearly be seen for Windemere 2008 and 2009 (Figs. 7a and 7d) and is most likely associated with inadequate representation of nutrient fluxes and subsequent periods of nutrient limitation (Page *et al*., 2017). There are also some periods where the overly rapid mixing simulated by the epilimnetic depth model (as discussed above) made it difficult to simulate the relatively high observed biomass: this is particularly evident for CS-species in Esthwaite Water 2008 (Fig. 7k) and R-species in Esthwaite Water 2009 (Fig. 7l); these inconsistencies are a direct result of the spurious deep mixing events simulated around days 220 and 250 for 2008 and 2009 respectively (see Fig. 2 b and c) and strengthen the requirement to improve the epilimnetic depth model as discussed above.

#### 3.2.4 Forecasting cyanobacteria

Observations of Cyanobacteria are estimated in the same way as functional species types discussed in the previous section and are associated with similar uncertainty (see Fig. 7). As PROTECH simulates the functional algal community using the dynamics of a number of selected individual species, the philosophy

behind this method means that the forecasts of individual species are not as robust as those for functional comuntity structure and are hence more uncertain. This is the case for forecasts of cyanobacteria where they are represented by more than one functional type: e.g. for Windermere cyanobacteria are represented by *Planktothrix*, an R-type species, together with *Aphanizomenon flos-aquae* and *dolichospermum* which are CS-type species (see Table Supp. 2). In this situation, the interchangeability of species with similar functional behaviour, but which have differing species traits, requires additional interpretation for forecasts of cyanobacteria to be made. For example, the simulations of the R-species *Planktothrix* for all lake-years for Windermere result in overestimations of cyanobacteria concentrations for the periods where *Planktothrix* proliferates (approximately between days 150 and 275: Figs. 7c, 7f & 7i). Cyanobacteria forecasts, made for this study, are also a spatial average for each lake, constrained using data collected at one point; they therefore do not necessarily correspond with the risk from cyanobacterial blooms where significant spatial heterogeneity exists, as can be the case for wind-blown cyanobacterial species (e.g. George and Heaney, 1978). Extending point forecasts to spatial forecasts for species that have these characteristics is hence an additional challenge. However, forecasts may be presented as probabilistic or possibilistic risk estimates, such as the likelihood of a cyanobacterial concentration of greater than a given critical threshold: this will be the focus of further research.

## 4 Conclusions

We rigorously tested the ability of the phytoplankton community model PROTECH to make forecasts of phytoplankton community structure within a data assimilation scheme using the Ensemble Kalman Filter. Some forecasting success was shown for chlorophyll *a*, but not all forecasts were better than a persistence forecast. The results typically indicated a reduction in chlorophyll *a* forecast skill with length of forecasting periodwith forecasts for up to four or five days showinggreater promise than those for longer time-scales. Associated forecasts of phytoplankton community composition, represented by functional algal types,

were broadly consistent with observations. Translation of forecasts of functional algal types to forecasts of cyanobacteria are challenging because of functional similarities between species which may or may not be cyanobacteria. Improvements in forecasts are likely to come from higher frequency observations for both chlorophyll *a* and nutrient concentrations. - While higher frequency observations for these variables should help improve forecasts, they will also simultaneously improve the persistence forecast. It, therefore, remains to be seen whether or not a modelled forecast driven with improved observations would provide a significant improvement over the associated persistence forecast and the potential to forecast algal blooms in this type of lake.

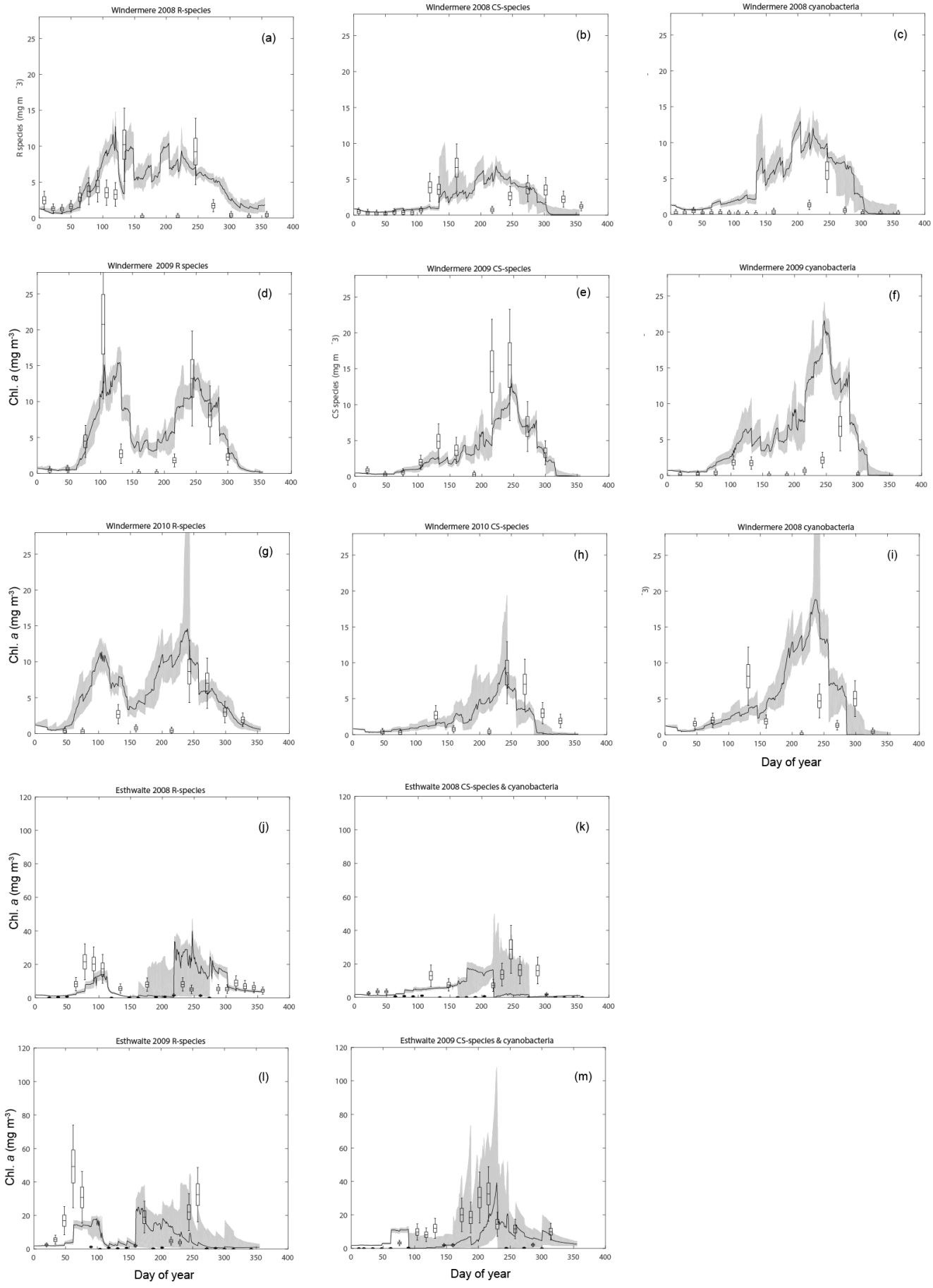
Windermere 2008 R-species
(a)
R species (mg m⁻³)
Windermere 2008 CS-species
(b)
Windermere 2008 cyanobacteria
(c)
Windermere 2009 R species
(d)
Chl. a (mg m⁻³)
Windermere 2009 CS-species
(e)
CS species (mg m⁻³)
Windermere 2009 cyanobacteria
(f)
Windermere 2010 R-species
(g)
Chl. a (mg m⁻³)
Windermere 2010 CS-species
(h)
Windermere 2008 cyanobacteria
(i)
Day of year
Esthwaite 2008 R-species
(j)
Chl. a (mg m⁻³)
Esthwaite 2008 CS-species & cyanobacteria
(k)
Esthwaite 2009 R-species
(l)
Chl. a (mg m⁻³)
Esthwaite 2009 CS-species & cyanobacteria
(m)
Day of year
Day of year

*Figure 7. Concatenated five-day ahead forecasts of R-species, CS-species and cyanobacteria concentration for all lake years; black line is 50$^{th}$ percentile and grey shaded area represents the 5$^{th}$ and 95$^{th}$ percentiles of the ensemble: EM200 and EM400 for Windermere and Esthwaite respectively*. The box and whisker symbols represent the analytical uncertainty and the total uncertainty estimated by the project team. Note that 5-day ahead forecasts are presented as approximately this lead time provided the most consistently acceptable results.

**Acknowledgements**

This work was supported by the Natural Environment Research Council projects: the United Kingdom Lake Ecological Observatory Network (UKLEON; grant number NE/I007407/1) and the Consortium on Risk in the Environment: Diagnostic, Integration, Benchmarking, Learning and Elicitation (CREDIBLE; grant number NE/J017299/1); We would like to thank the ECMWF for the historic meteorological forecasts and Mr Bernard Tebay for collecting the meteorological data at Ambleside.

**References**

Anderson, J.L. (2007). An adaptive covariance inflation error correction algorithm for ensemble filters. Tellus, 59A, 210–224

Anderson, J.L., Anderson, S.L. (1999). A Monte Carlo implementation of the nonlinear filtering problem to produce ensemble assimilations and forecasts. Mon. Wea. Rev. 127, 2741–2758.

J. Allen, M. Eknes, G. Evensen. (2003). An Ensemble Kalman Filter with a complex marine ecosystem model: hindcasting phytoplankton in the Cretan Sea. Ann. Geophys., 21, 399–411.

550 Bennion, H., Monteith, D. and Appleby, P. (2000). Temporal and geographical variation in lake trophic
551 status in the English Lake District: evidence from (sub)fossil diatoms and aquatic macrophytes. Freshwater
552 Biol., 45(4), 1365-2427, doi: 10.1046/j.1365-2427.2000.00626.x

553 Buizza, R., Milleer, M. and Palmer, T. N. (1999). Stochastic representation of model uncertainties in the
554 ECMWF ensemble prediction system. Q. J. Roy. Meteor. Soc. 125 (560), 2887–2908.
555 doi:10.1002/qj.49712556006.

556 Carmichael, W.W. (1992). A status report on planktonic cyanobacteria (blue-green algae) and their toxins.
557 EPA/600/R-92-079, Environmental Monitoring Systems Laboratory, Office of Research and Development,
558 U.S. Environmental Protection Agency, Cincinnati, OH. 141 pp.

559 Dong X., Bennion H., Maberly S.C., Sayer C.D., Simpson G.L. and Battarbee R.W. (2012). Nutrients provide
560 a stronger control than climate on diatom communities in Esthwaite Water Water: Evidence from
561 monitoring and palaeolimnological records over the past 60 years. Freshwater Biol., 57, 2044-2056.

562 Elliott, J.A. (2012) Predicting the impact of changing nutrient load and temperature on the phytoplankton
563 of England's largest lake, Windermere. Freshwater Biol., 57, 400-413.

564 Elliott, J.A. (2010). The seasonal sensitivity of Cyanobacteria and other phytoplankton to changes in
565 flushing rate and water temperature. Glob. Change Biol., 16, 864-876.

566 Evensen, G. (1994). Sequential data assimilation with a non-linear quasigeostrophic model using Monte
567 Carlo methods to forecast error statistics. J. Geophys. Res., 99, 10 143–10 162.

568 Evensen, G. (2009). The ensemble Kalman filter for combined state and parameter estimation. IEEE
569 Control Sys., 29 (3), pp. 83-104, 2009.

George, D. G. and Heaney, S. I. (1978). Factors influencing the spatial distribution of phytoplankton in a small productive lake. J. Ecol., 66(1), 133-155.

Hall, G.H., Maberly, S.C., Reynolds, C.S., Winfield, I.J., James, B.J., Parker, J.E., Dent, M.M., Fletcher, J.M., Simon, B.M. and Smith, E. (2000). Feasibility study on the restoration of three Cumbrian lakes. Centre for Ecology and Hydrology Windermere, Ambleside, UK. 82 pp.

Heany, S.I., Corry, J. E. and Lishman, J. P. (1992). Changes of water quality and sediment phosphorus of a small productive lake following decreased phosphorus loading. Centre for Ecology and Hydrology Windermere, Ambleside, UK. 14 pp.

Ho, J. C. and Michalak, A. M. (2015). Challenges in tracking harmful algal blooms: A synthesis of evidence from Lake Erie. J. Great Lakes Res., 41(2), 317-325. doi.org/10.1016/j.jglr.2015.01.001

Huang, J., Gao, J., Liu, J. and Zhang, Y. (2013). State and parameter update of a hydrodynamic-phytoplankton model using ensemble Kalman filter, Ecol. Model., 263 (10), 81-91. https://doi.org/10.1016/j.ecolmodel.2013.04.022

Kim, K., Park, M., Min, J., Ryu, I., Kang, M., and Park, L. (2014). Simulation of algal bloom dynamics in a river with the ensemble Kalman filter. J. Hydrol., 519(D), 2810–2821. https://doi.org/10.1016/j.jhydrol.2014.09.073

Luo, Y., Ogle, K., Tucker, C., Fei, S., Gao, C., LaDeau, S., Clark, J. S. and Schimel, D. S. (2011). Ecological forecasting and data assimilation in a data-rich era. Ecol. Appl., 21, 1429–1442. doi:10.1890/09-1275.1

Maberly, S.C., De Ville, M.M., Thackeray, S.J., Feuchtmayr, H., Fletcher, J.M.,James, J.B., Kelly, J.L., Vincent, C.D., Winfield, I.J., Newton, A., Atkinson, D., Croft,A., Drew, H., Saag, M., Taylor, S., Titterington, H. (2011). A survey of the lakes of the English Lake District: The Lakes Tour 2010. NERC/Centre for Ecology and Hydrology,137pp. (CEH Project Number. Report to: Environment Agency, North West Region and Lake

592 District National Park Authority: downloaded Jan 2015 from
593 http://nora.nerc.ac.uk/14563/2/N014563CR.pdf

594 Mackay E. M., Folkard A. M. and Jones I.D. (2014). Interannual variations in atmospheric forcing determine
595 trajectories of hypolimnetic soluble reactive phosphorus supply in a eutrophic lake. Freshwater Biol., 59,
596 1646–1658.

597 Madgwick G., Jones I.D., Thackeray S.J., Elliott J.A. and Miller H.J. (2006). Phytoplankton communities and
598 antecedent conditions: high resolution sampling in Esthwaite Water Water. Freshwater Biol., 51, 1798–
599 1810.

600 Marcé, R., George, G., Buscarinu, P., Deidda, M, Dunalska, J., de Eyto, E., Flaim, G., Grossart, H.,
601 Istvanovics, V., Lenhardt, M., Moreno-Ostos, E., Obrador, B., Ostrovsky, I., Pierson, D. C., Potužák, J.,
602 Poikane, S., Rinke, K., Rodríguez-Mozaz, S., Staehr, P. A., Šumberová, K., Waajen, G., Weyhenmeyer, G. A.,
603 Weathers, K. C., Zion, M., Ibelings, B.W. and Jennings, E. (2016). Automatic High Frequency Monitoring
604 for Improved Lake and Reservoir Management. Environ. Sci. Technol. 50 (20), 10780-10794. DOI:
605 10.1021/acs.est.6b01604

606 Michalak, A., M. (2016). Study role of climate change in extreme threats to water quality. Nature 535, 349-
607 350.

608 Metcalf, J.S. and Codd, G.A. (2009). Cyanobacteria, neurotoxins and water resources: are there
609 implications for human neurodegenerative disease? Amyotrophic Lateral Sclerosis 10, suppl. 2, 74-78
610 (2009).

611 Moradkhani, H., S. Sorooshian, H. V. Gupta, and P. R. Hauser (2005). Dual state-parameter estimation of
612 hydrological models using ensemble Kalman filter, Adv. Water Resour., 28, 135 – 147.

Ollinaho, P., Lock, S.-J., Leutbecher, M., Bechtold, P., Beljaars, A., Bozzo, A., Forbes, R. M., Haiden, T., Hogan, R. J. and Sandu, I. (2017), Towards process-level representation of model uncertainties: stochastically perturbed parametrizations in the ECMWF ensemble. Q.J.R. Meteorol. Soc., 143: 408–422. doi:10.1002/qj.2931

Page et al., (2017). Constraining uncertainty and process-representation in an algal community lake model using high frequency in-lake observations. Ecol. Model.: http://www.sciencedirect.com/science/article/pii/S0304380017301345

Paerl, H.W. and Huisman, J. (2008). Blooms like it hot. Science, 4, 320(5872), 57-8. doi: 10.1126/science.1155398. DOI: 10.1126/science.1155398

Pretty, J. N., Mason, C. F., Nedwell, D. B., Hine, R. E., Leaf, S., and Dils, R. (2003). Environmental Costs of Freshwater Eutrophication in England and Wales. Environ. Sci. Technol., 37(2), 201-208.

Read J.S., Hamilton, D.P., Jones, I.D., Muraoka, K., Winslow, L.A. , Kroiss, R. , Wu, C.H. & Gaiser. E. (2011). Derivation of lake mixing and stratification indices from high-resolution lake buoy data. Environ. Modell. Softw. 26, 1325-1336.

Ramsbottom A.E. (1976). Depth Charts of the Cumbrian Lakes. Freshwater Biological Association Scientific Publication No. 33, Ambleside, UK.

Recknagel, F., Ostrovsky, I. and Cao, H. (2014). Model ensemble for the simulation of plankton community dynamics of Lake Kinneret (Israel) induced from in situ predictor variables by evolutionary computation. Environ. Modell. Soft., 61, 380-392. https://doi.org/10.1016/j.envsoft.2014.03.014.

Reynolds C.S. (1988). Functional morphology and the adaptive strategies of freshwater phytoplankton. In: Growth and Reproductive strategies of Freshwater Phytoplankton (Ed. C.D. Sandgren), pp. 388–433. Cambridge, University Press, New York.

635 Reynolds C.S., Irish A.E. and Elliott J.A. (2001). The ecological basis for simulating phytoplankton responses
636 to environmental change (PROTECH). Ecol. Model., 140, 271–291.

637 Rigosi, A., Carey, C.C., Ibelings, B. W. and Brookes, J. D. (2014). The interaction between climate warming
638 and eutrophication to promote cyanobacteria is dependent on trophic state and varies among taxa.
639 Limnol. Oceanogr. 59(1), 2014, 99–114. doi:10.4319/lo.2014.59.01.0099

640 Rowe, M. D., Anderson, E. J. , Wynne, T. T., Stumpf, R. P., Fanslow, D. L., Kijanka, K., Vanderploeg, H. A.
641 Strickler, J. R. and Davis, T. W. (2016). Vertical distribution of buoyant Microcystis blooms in a Lagrangian
642 particle tracking model for short-term forecasts in Lake Erie. J. Geophys. Res.: Oceans. 121, 5296-5314.
643 doi:10.1002/2016JC011720.

644 Smith, V.H., (2003). Eutrophication of Freshwater and Coastal Marine Ecosystems: A Global Problem.
645 Environ. Sci. & Pollut. Res. 10 (2) 126-39.

646 Stumpf, R. P., Tomlinson, M. C., Calkins, J. A., Kirkpatrick, B., Fisher, K., Nierenberg, K., Currier, R. and
647 Wynne, T. T. (2009). Skill assessment for an operational algal bloom forecast system. Journal of Marine
648 Systems. 76(1): 151-161.

649 Taylor, C.J., Pedregal, D.J., Young, P.C. and Tych, W., (2007). Environmental time series analysis and
650 forecasting with the Captain toolbox, Environ. Modell. Softw., 22: 797-814.

651 World Health Organization (1999). Toxic cyanobacteria in water: a guide to their public health
652 consequences, monitoring and management. I. Chorus and J. Bartram (Eds.). E & FN Spon, London, UK
653 (1999).

654

Xiao X, Sogge H, Lagesen K, Tooming-Klunderud A, Jakobsen KS, Rohrlack T (2014). Use of High Throughput Sequencing and Light Microscopy Show Contrasting Results in a Study of Phytoplankton Occurrence in a Freshwater Environment. PLoS ONE, 9(8), 1-9. doi:10.1371/journal.pone.0106510

Xiao, X., He, J., Huang, H., Miller, T. R., Christakos, G., Reichwaldt, E., S., Ghadouani, A., Lin, S., Xu, X. and Shi, J. (2017). A novel single-parameter approach for forecasting algal blooms. Water Res., 108, 222-231. https://doi.org/10.1016/j.watres.2016.10.076

Young, P.C. and Beven, K.J. 1994. Data-based mechanistic modelling and the rainfall-flow non-linearity. Environmetrics. 5, 3, p. 335-363.

Ye, L., Cai, Q., Zhang, M. and Tan, L. (2014). Real-time observation, early warning and forecasting phytoplankton blooms by integrating in situ automated online sondes and hybrid evolutionary algorithms. Ecological Informatics, 22, 44–51.

Young, P.C., 2015. Refined Instrumental Variable Estimation: Maximum Likelihood Optimization of a Unified Box-Jenkins Model. Automatica, 52, 35–46.

**Supplementary information**

**Supp. 1 Transfer Function models for forecasted inputs**

The epilimnetic depth model requires forecasts of epilimnetic temperature, river in/outflows and river temperature. Each TF model that provides these forecasts was identified (as outlined above) using the available timeseries data. The epilimnetic temperature ($T_e$) at day *t* is given by:

$$T_{e(t)} = -a.T_{e\,(t-1)} b1.T_{a(t)} + b2.R_{sw(t)} + b3.\frac{1}{D_{e(t-1)}} + b4.\left(W_{s(t-1)}\right)^3$$

676

677

678 Where, $T_a$ is the air temperature, $R_{sw}$ is SW radiation, $D_e$ is epilimnetic depth and $W_S$ is the wind speed.
679 The model coefficients are denoted *a*, *b1*, *b2* and *b3* (see Table Supp. 1 for values). One model for each
680 lake was identified from the available data (2008 to 2010 for Windermere and 2004 to 2009 for Esthwaite
681 Water).

682 The lake in/outflow TF model was identified as a 1st order model with a nonlinear rainfall filter (see Young
683 and Beven, 1994) and took the form:

684

685 $$Q_{r(t)} = -a.Q_{r(t-1)} + b.P_{(t)}.Q_{r(t-1)}{}^{\beta}$$

686

687

688 where $Q_r$ is the river in/outflow, *P* is precipitation and *a*, *b1* are TF model coefficients where $\beta$ is the
689 nonlinear rainfall filter parameter. The model for Windermere was identified using Rainfall data from
690 Ambleside and flow data from the Environment agency Gauge at Newby Bridge for the years 2008 to 2010
691 (National River Flow Archive: http://www.ceh.ac.uk/data/nrfa/).

692 River temperature ($T_Q$) was estimated using observed data from Troutbeck (Windermere) for the years
693 1997 to 2006:

694

695 $$T_{Q(t)} = -a.T_{Q(t-1)} + b.T_{a(t)}$$

696

697

698

699 ***Table Supp. 1 Transfer Function parameters and goodness of fit (W = Windermere; E = Esthwaite Water)***

| | a | | b1 ($\beta$) | | b2 | | b3 | | b4 | | τ | | $R_T^2$ | |
|---|---|---|---|---|---|---|---|---|---|---|---|---|---|---|
| | **W** | **E** | **W** | **E** | **W** | **E** | **W** | **E** | **W** | **E** | **W** | **E** | **W** | **E** |
| Lake Surface Temperature ($T_s$) | -0.9449 | -0.899 | 0.055 | 0.093 | 0.0008 | 0.0025 | 0.0011 | 0.0022 | -0.0007 | -0.0012 | [0,0,0,0] | [0,1,1,0] | 0.97 | 0.98 |
| River in/outflow ($Q_r$) | -0.7717 | -0.829 | 11.141 (0.2) | 0.022 (0.3) | | | - | - | | | 1 | 0 | 0.92 | 0.86 |
| River Temperature ($T_Q$) | -0.900 | -0.900 | 0.1005 | 0.1005 | - | - | - | - | - | - | 0 | 0 | 0.87 | 0.87 |

700

701 ***Table Supp. 2. Species used to represent algal communities. Functional algal types and an indication of***
702 ***classification as cyanobacteria given are in parenthesis: functional types follow*** **Reynolds (1988).**

| **Windermere** | **Esthwaite Water Water** |
|---|---|
| *Aphanizomenon flos-aquae (CS; Cyano)* | *Asterionella (R)* |
| *Aulacoseira (R)* | *Aulacoseira* - 2008 *(R)*; *Fragilaria crotonensis-(2009 (R)* |
| *Asterionella (R)* | *Aphanizomenon flos-aquae (CS; Cyano)* |
| *Cryptomonas (CSR)* | *Aphanothece clathrata (CS; Cyano)* |
| *Dolichospermum (CS; Cyano)* | *Cryptomonas (CSR)* |
| *Monoraphidium (CS)* | *Dictyosphaerium pulchellum (R)* |
| *Paulschulzia tenera (S)* | *Dolichospermum (CS; Cyano)* |
| *Planktothrix (R; Cyano)* | *Eudorina (S)* |

703